Check for updates

ADVANCED MATERIALS
www.advmat.de

Judicious Heteroatom Doping Produces High-Performance Deep-Blue/Near-UV Multiresonant Thermally Activated Delayed Fluorescence OLEDs

Subeesh Madayanad Suresh, Le Zhang, Tomas Matulaitis, David Hall, Changfeng Si, Gaetano Ricci, Alexandra M. Z. Slawin, Stuart Warriner, David Beljonne, Yoann Olivier, Ifor D. W. Samuel, and Eli Zysman-Colman**

Two multiresonant thermally activated delayed fluorescence (MR-TADF) emitters are presented and it is shown how further borylation of a deep-blue MR-TADF emitter, DIDOBNA-N, both blueshifts and narrows the emission producing a new near-UV MR-TADF emitter, MesB-DIDOBNA-N, are shown. DIDOBNA-N emits bright blue light (Φ_{PL} = 444 nm, FWHM = 64 nm, Φ_{PL} = 81%, τ_d = 23 ms, 1.5 wt% in TSPO1). The deep-blue organic light-emitting diode (OLED) based on this twisted MR-TADF compound shows a very high maximum external quantum efficiency (EQE_{max}) of 15.3% for a device with CIE_y of 0.073. The fused planar MR-TADF emitter, MesB-DIDOBNA-N shows efficient and narrowband near-UV emission (λ_{PL} = 402 nm, FWHM = 19 nm, Φ_{PL} = 74.7%, τ_d = 133 ms, 1.5 wt% in TSPO1). The best OLED with MesB-DIDOBNA-N, doped in a co-host, shows the highest efficiency reported for a near-UV OLED at 16.2%. With a CIE_y coordinate of 0.049, this device also shows the bluest EL reported for a MR-TADF OLED to date.

1. Introduction

Organic light-emitting diodes (OLEDs) are rapidly becoming the preferred display technology for a range of consumer electronics, from smartwatches, mobile phones, and laptops to large-screen televisions and displays used in the automotive industry.[1] Ultrahigh-definition displays must meet ever more stringent industry color standards, the most recent of which being Rec 2020, which are defined according to the Commission International de l'Éclairage (CIE) 1931 as (0.131, 0.046), (0.17, 0.797) and (0.708, 0.292) for blue, green and red, respectively.[2] Presently commercial vacuum-deposited OLEDs rely on phosphorescent complexes as emitter materials for the red and green sub-pixels and organic fluorescent materials for the blue sub-pixel. Significant research has been devoted to developing sustainable organic emitters that operate at comparable efficiencies to phosphorescent complexes and so can replace noble-metal-based emitters for red and green OLEDs, and for blue OLEDs can lead to much higher efficient devices.[3] Organic compounds that exhibit thermally activated delayed fluorescence (TADF) have the most potential to act as replacement emitters in OLEDs as this class of material

S. M. Suresh, L. Zhang, T. Matulaitis, D. Hall, C. Si, A. M. Z. Slawin, E. Zysman-Colman
Organic Semiconductor Centre
EaStCHEM School of Chemistry
University of St Andrews
St Andrews KY16 9ST, UK
E-mail: eli.zysman-colman@st-andrews.ac.uk

L. Zhang, I. D. W. Samuel
Organic Semiconductor Centre
SUPA School of Physics and Astronomy
University of St Andrews
St Andrews KY16 9SS, UK
E-mail: idws@st-andrews.ac.uk

D. Hall, D. Beljonne, Y. Olivier
Laboratory for Chemistry of Novel Materials
University of Mons
Mons 7000, Belgium

G. Ricci, Y. Olivier
Laboratory for Computational Modeling of Functional Materials
Namur Institute of Structured Matter
Université de Namur
Rue de Bruxelles, 61, Namur 5000, Belgium

S. Warriner
School of Chemistry
University of Leeds
Woodhouse Lane, Leeds LS2 9JT, UK

The ORCID identification number(s) for the author(s) of this article can be found under https://doi.org/10.1002/adma.202300997

© 2023 The Authors. Advanced Materials published by Wiley-VCH GmbH. This is an open access article under the terms of the Creative Commons Attribution License, which permits use, distribution and reproduction in any medium, provided the original work is properly cited.

DOI: 10.1002/adma.202300997

15214095, 2023, 33, Downloaded from https://onlinelibrary.wiley.com/doi/10.1002/adma.202306997 by Universite De Mons (Umons), Wiley Online Library on [21/08/2023]. See the Terms and Conditions (https://onlinelibrary.wiley.com/terms-and-conditions) on Wiley Online Library for rules of use; OA articles are governed by the applicable Creative Commons License

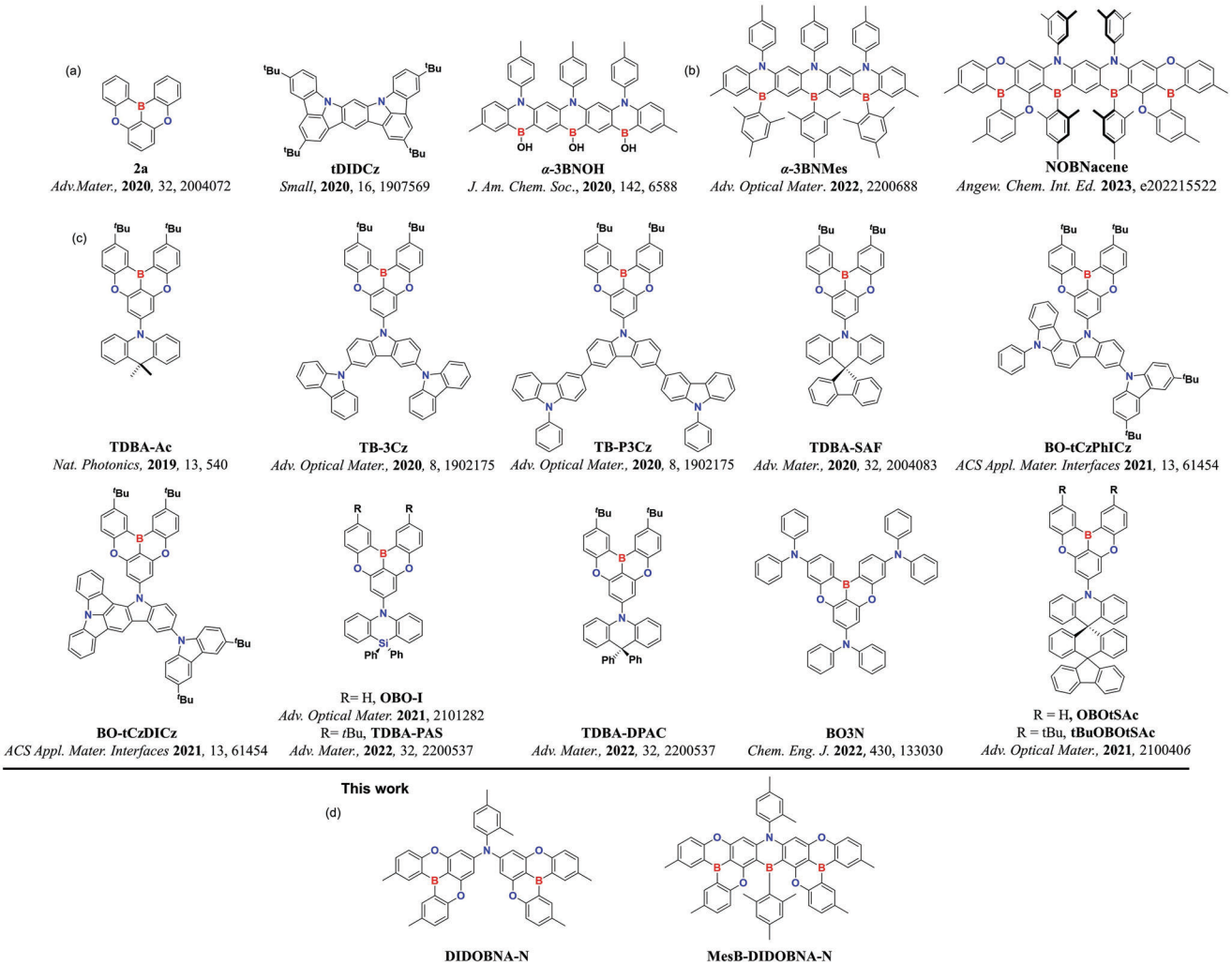

Figure 1. a) Chemical structures of previously reported near-UV MR-TADF emitters, b) α-3BNMes and NOBNacene, c) D–A TADF emitters with $CIE_y \leq 0.1$ with a DOBNA acceptor fragment, and d) chemical structures of the emitters presented in this work.

can harvest 100% of the electrically generated excitons and convert these to light emission.[4] Though TADF OLEDs now show comparable efficiencies to phosphorescent OLEDs for each of the red, green, and blue devices, the typically employed donor–acceptor (D–A) design results in emission from a charge-transfer (CT) state that is broad and unstructured, leading to poor chromaticity in the device. A subclass of TADF emitters, multiresonant TADF (MR-TADF), however, shows great promise to address the issue of color purity. MR-TADF emitters show very narrow-band emission (full-width half maximum (FWHM) < 40 nm),[5] which is due to their very rigid polycyclic aromatic structure and their short-range charge transfer (SRCT) excited state.[6] Their use in OLEDs would obviate the need for the use of color filters, leading to more energy-efficient devices.

Since the first report of an MR-TADF compound from the group of Hatakeyama, over two hundred separate MR-TADF materials have been identified as hosts or emitters for OLEDs,[6a,7] with examples of their use in high-efficiency blue, green and red OLEDs. Near-UV emitters for OLEDs are one class where there is a dearth of reports.[8] Potential uses of short wavelength OLEDs are for sensing,[9] photocopying,[10] high-density information storage,[11] and sterilization.[12] Most of the reported efficient near-UV OLEDs (<400 nm) using purely organic emitters[8] to date contain materials that emit from a hybridized local and charge transfer excited state (HLCT)[13] where triplets are harvested through a hot exciton channel mechanism involving reverse intersystem crossing (RISC) from higher lying triplet (T_n) states to S_1.[14] A recent report from Tang et al. demonstrated record-setting performance values for an hybridized local and charge transfer (HLCT) emitter-based near-UV OLED (λ_{EL} = 396 nm, EQE_{max} = 10.79%, CIE (0.161, 0.031)).[3a,6a,8] There are also a small number of reports of near-UV TADF and MR-TADF emitters and their use in OLEDs (**Figure 1**).[7] The first report of a near-UV-emitting MR-TADF compound is based on a boron, oxygen doped triangulene type structure reported by Hatakeyama, 2a[15] (λ_{PL} = 398 nm, FWHM = 33 nm, ΔE_{ST} = 0.18 eV, τ_d = 66 µs in 1 wt% poly(methyl methacrylate) (PMMA).[16] This compound, also known as DOBNA, was initially identified as a potential host material due to its large band gap and high triplet energy. In the same report, phenyl derivatives of 2a were

 © 2023 The Authors. Advanced Materials published by Wiley-VCH GmbH

employed as host materials in phosphorescent OLEDs.[15] Other reports have mostly documented the use of the DOBNA fragment as a weak acceptor in D–A type near-UV[17] (λ_{PL} < 450 nm) TADF emitters.[6a] In 2015, Kwon et al. reported two deep-blue emitters containing the DOBNA fragment as the acceptor.[18] The OLED with the acridine donor-based emitter, TDBA-Ac presented an maximum external quantum efficiency (EQE_{max}) of 21.5% and an excellent CIE_y of 0.06. Choi et al. reported devices using related tercarbazole donor-based TB-3Cz and TB-P3Cz emitters that showed EQE_{max} of 9.9% and 6.1%, respectively, with corresponding CIE_y values were 0.07 and 0.08, respectively, for TB-3Cz and TB-P3Cz.[19] A structurally related deep-blue emitter containing a spiroacridan donor was reported by Kim et al., TDBA-SAF-based device achieved an EQE_{max} of 28.2% and a CIE_y of 0.09.[20] Recently, Choi et al. reported two deep-blue solution-processible emitters containing extended carbazole donor units connected to DOBNA acceptor, BO-tCzPhICz and BO-tCzDICz. The solution-processed OLEDs showed EQE_{max} of 17.8% and 14.8%, respectively, and with CIE_y of 0.07 and 0.062, respectively.[21] Hong et al. reported two tri-spiral acridine donor-based blue emitters, OBOtSAc and tBuOBOtSAc, and their use in OLEDs.[22] Both emitters showed efficient (Φ_{PL} above 90%) deep-blue emission at 452 (FWHM = 50 nm) and 446 nm (FWHM = 48 nm), respectively, for OBOtSAc and tBuOBOtSAc. Both devices achieved very high EQE_{max} of 31.2% and 28.2% with CIE_y of 0.092 and 0.061, respectively. Tong et al. reported OLEDs using two deep-blue emitters TDBA-PAS and TDBA-DPAC that can achieve EQE_{max} of 22.4% and 24.6% at CIE_y of 0.042 and 0.085, respectively.[23] These two emitters each show two different conformers in the solid state and the authors contend that one conformer acts as a host for the other, evidenced by the improved performance in the device at high doping concentrations (≤50 wt%). Su et al. reported a disk-like emitter based on a DOBNA acceptor decorated with three diphenylamine units, BO3N, which showed narrowband blue emission (λ_{PL} = 424 nm, FWHM = 34 nm) with high Φ_{PL} of 80% in toluene solution. The OLED with the emitter BO3N showed an EQE_{max} of 10.4% and CIE_y value of 0.08.[24]

The DOBNA fragment has thus been shown to be a promising motif used in the construction of D–A type efficient deep-blue TADF emitters, though it is still challenging to tune the emission wavelength further to the near-UV region (i.e., around 400 nm). An alternative design for UV emitters was highlighted by Lee et al. where they reported a fused indolocarbazole (tDIDCz) derivative that presented incredibly narrowband EL (FWHM = 14 nm, λ_{EL} = 401 nm) with CIE coordinates of (0.164, 0.018) in the device.[25] Though this compound shows the characteristic pattern of alternating increasing and decreasing electron density on adjacent atoms in the excited state, the ΔE_{ST} of 0.44 eV is too large due to the very different natures of the S_1 and T_1 excited states resulting in the absence of delayed fluorescence.[26] The absence of triplet harvesting in the OLED limited the EQE_{max} to only 2.75% (Table S7, Supporting Information).

In 2020, we reported a near-UV-emitting linear ladder type B,N-doped heptacene (Figure 1), α-3BNOH (λ_{PL} = 390 nm, FWHM = 31 nm, ΔE_{ST} = 0.31 eV in THF), that showed an emission resulting from TADF and TTA and narrow deep-blue emission in solution.[27] By replacing the OH group attached to boron with mesityl units in α-3BNOH, a redshift of the emission was observed for α-3BNMes (λ_{PL} = 443 nm, FWHM = 30 nm, THF, ΔE_{ST} = 0.28 eV, 1 wt% in PMMA).[28] In 2023, we reported a deep-blue heteroatom-doped nonacene derivative, NOBNacene.[29] The OLED with this emitter showed deep-blue electroluminescence (λ_{EL}, of 412 nm, FWHM of 41 nm) with an EQE_{max} of 11.2%. Here, we report two emitters MR-TADF emitters, one is twisted, containing two DOBNA groups and a bridging amine that emits in the deep blue (DIDOBNA-N), and a second fused planar B,N,O doped heptacene compound that emits in the near-UV (MesB-DIDOBNA-N). Both compounds exhibit weak TADF due to their moderately large ΔE_{ST} of 0.23 and 0.24 eV yet demonstrate high Φ_{PL} of 81 and 73% for DIDOBNA-N and MesB-DIDOBNA-N, respectively in doped films. The OLED with DIDOBNA-N showed deep-blue emission at 444 nm (FWHM = 64 nm) corresponding to CIE coordinates of (0.152, 0.073) with an EQE_{max} of 15.2%. The OLED with MesB-DIDOBNA-N showed narrowband near-UV emission with λ_{EL} of 402 nm, FWHM = 21 nm, corresponding to CIE coordinates of (0.170, 0.049). The EQE_{max} value of the 3 wt% emitter-doped in a co-host device represents the most efficient device among those employing purely organic near-UV emitters.[7,8] and represents record-breaking device performance value for a near-UV MR-TADF OLED device reported to date.[30]

2. Results and Discussion

MesB-DIDOBNA-N was obtained in three steps from compound 1 (**Figure 2**). DOBNA-Br, a key intermediate, was obtained through a sequence of S_NAr and electrophilic borylation in good yield; the borylation reaction proceeded in 73% yield. DIDOBNA-N was obtained in 57% yield following a Buchwald–Hartwig cross-coupling reaction of two equivalents of DOBNA-Br with 2,4-dimethylaniline. DIDOBNA-N was then subjected to electrophilic borylation with BBr_3 and quenching with MesMgBr to afford MesB-DIDOBNA-N in 74% yield. The identity and purity of the synthesized molecules were established from a combination of ^{1}H and ^{13}C NMR spectroscopy, high-resolution mass spectrometry (HRMS), elemental analysis (EA), and gel permeation chromatography (GPC) (Figures S1–S15, Supporting Information)

Single crystals of DOBNA-Br were obtained directly from the reaction mixture. DIDOBNA-N crystals were obtained following temperature-gradient sublimation, and MesB-DIDOBNA-N were obtained by slow diffusion of hexane into a saturated solution of the emitter in THF. Their structures are shown in Figure 2b–d. No intermolecular hydrogen bonding or π–π stacking interactions were observed for DIDOBNA-N and MesB-DIDOBNA-N. In MesB-DIDOBNA-N, the B—C_{Mes} bond is longer (1.587(3) Å) than the B–C bonds within the DOBNA fragment (1.536(3) and 1.540(3) Å), a structural feature previously observed in other compounds containing a mesitylated borane.[31] This emitter has a planar structure and the two aryl moieties attached to the B and N positioned are oriented approximately orthogonal to the acene core. DIDOBNA-N adopts a twisted structure in the crystal.

We then undertook a computational study to understand the ground and excited state properties of both emitters (**Figure 3**). Ground state calculations were carried out using density functional theory (DFT) at the PBE0/6-31G(d,p) level in the gas phase. The DFT calculations predict a 0.12 eV increase in the band gap from DIDOBNA-N to MesB-DIDOBNA-N, despite the apparent

© 2023 The Authors. Advanced Materials published by Wiley-VCH GmbH

15214095, 2023, 33, Downloaded from https://onlinelibrary.wiley.com/doi/10.1002/adma.202300997 by Universite De Mons (Umons), Wiley Online Library on [21/08/2023]. See the Terms and Conditions (https://onlinelibrary.wiley.com/terms-and-conditions) on Wiley Online Library for rules of use; OA articles are governed by the applicable Creative Commons License

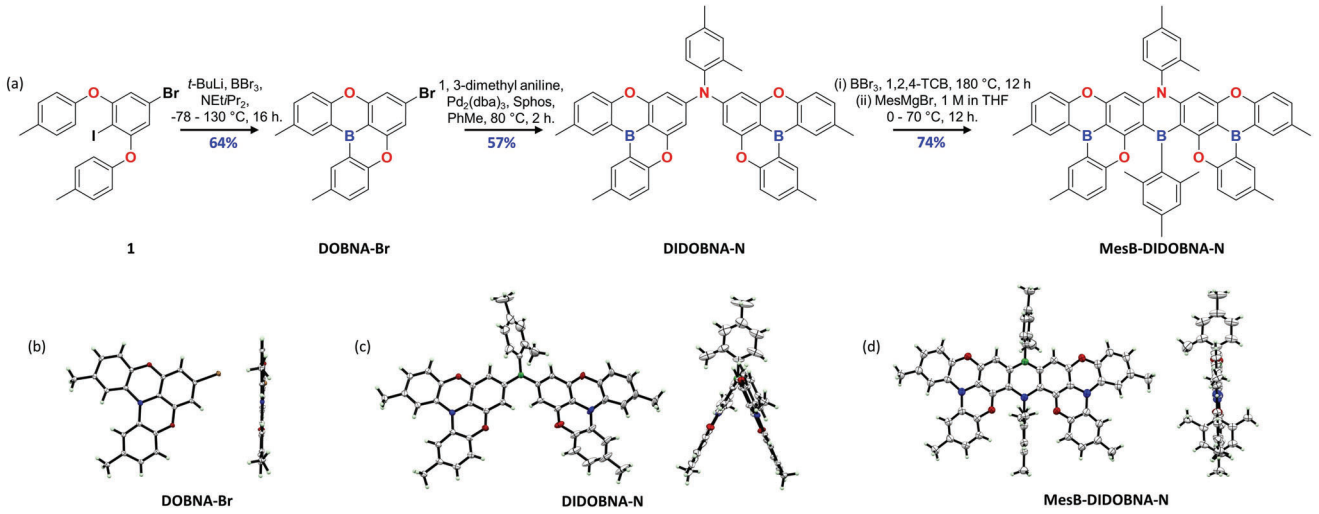

Figure 2. a) Synthesis of target emitters. b–d) ORTEP diagram of compounds, and their side views for Br-DOBNA (b), DIDOBNA-N (c), and MesB-DIDOBNA-N (d). Thermal ellipsoids are displayed at the 50% probability level.

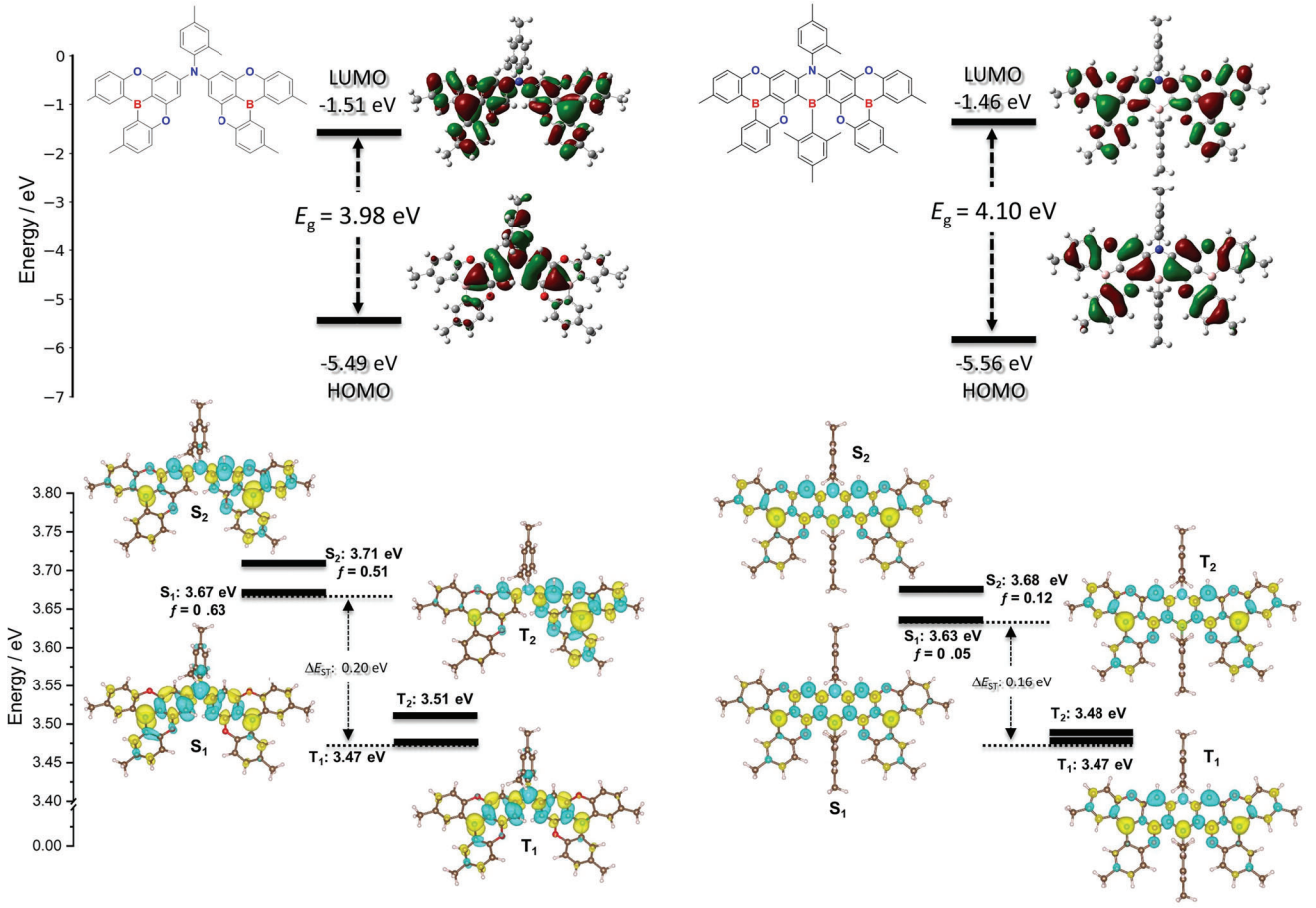

Figure 3. a) HOMO and LUMO electron density distribution and orbital energies of DIDOBNA-N and MesB-DIDOBNA-N calculated at PBE0/6-31G(d,p) in the gas phase, isovalue = 0.02; b) difference density plots and energies for the two lowest lying singlet and triplet excited states for DIDOBNA-N and MesB-DIDOBNA-N calculated at SCS-CC2/cc-pVDZ in the gas phase (isovalue = 0.001). Blue color represents an area of decreased electron density, and yellow represents an increased electron density between the ground and excited states. *f* denotes the oscillator strength for the transition to the excited singlet state.

 © 2023 The Authors. Advanced Materials published by Wiley-VCH GmbH

15214095, 2023, 33, Downloaded from https://onlinelibrary.wiley.com/doi/10.1002/adma.202300997 by Universite De Mons (Umons), Wiley Online Library on [21/08/2023]. See the Terms and Conditions (https://onlinelibrary.wiley.com/terms-and-conditions) on Wiley Online Library for rules of use; OA articles are governed by the applicable Creative Commons License

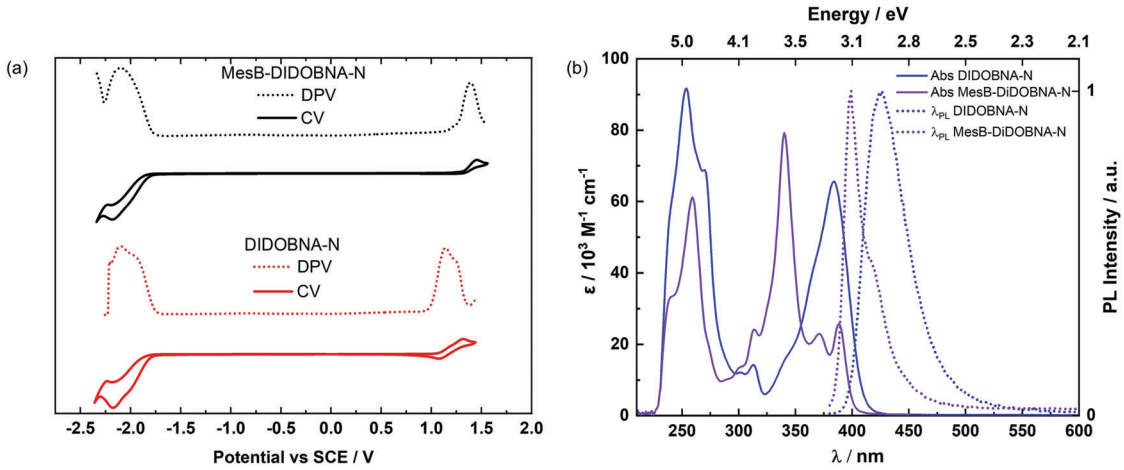

Figure 4. a) Cyclic and differential pulse voltammograms measured in degassed DCM with 0.1 M $[^nBu_4N]PF_6$ as the supporting electrolyte and Fc^+/Fc as the internal reference (0.46 V vs SCE).[35] Scan rate = 50 mV s^{-1}. b) Solution-state absorption and steady-state emission spectra at 300 K measured in THF. λ_{exc} = 365 nm.

increase in conjugation length. Both DIDOBNA-N and MesB-DIDOBNA-N display similar electron density distribution patterns for their LUMOs, with a pattern that is reminiscent of the DOBNA moiety[15] (Figure S16, Supporting Information). However, DIDOBNA-N and MesB-DIDOBNA-N show distinct electron density distribution patterns for their HOMOs. The electron density of the HOMO in DIDOBNA-N is reminiscent of triphenylamine, a good electron donor, while the electron density of the HOMO in MesB-DIDOBNA-N is localized on the DOBNA units, similar to the DOBNA core,[15] and with a nodal plane passing through the central nitrogen and boron atoms of the molecule. Excited state calculations were performed using wave-function-based methods using the spin-component scaling second-order approximate coupled-cluster (SCS-CC2) in tandem with the cc-pVDZ basis set, which we have previously shown to be a sufficient level of theory to accurately predict ΔE_{ST} in MR-TADF emitters.[32] The S_1 energy of DIDOBNA-N of 3.67 eV is slightly higher than that of MesB-DIDOBNA-N at 3.63 eV. Despite their similar S_1 energies, the oscillator strengths (f) for the S_0–S_1 transition are starkly different at 0.63 and 0.05 for DIDOBNA-N and MesB-DIDOBNA-N, respectively. The much-attenuated f in MesB-DIDOBNA-N is likely the result of the higher symmetry of this compound (Figure S17, Supporting Information). Notably, a similar change in the properties of the singlet excited state was predicted for DABNA-1 compared to its more symmetric fused derivative TABNA.[32] Identical T_1 energies of 3.47 eV were predicted for DIDOBNA-N and MesB-DIDOBNA-N, resulting in ΔE_{ST} of 0.20 and 0.16 eV, respectively. An intermediate triplet state was predicted to exist in both compounds, which is acknowledged to facilitate RISC via spin-vibronic coupling in D–A TADF emitters.[32,33] Difference density plots of the S_1, S_2, T_1, and T_2 states are shown in Figure 2b. Both compounds show excited states with the typical alternating pattern of increasing and decreasing electron density of MR-TADF compounds that is characteristic of an excited state possessing SRCT character. The magnitude of the CT character of the excited state was quantified using two separate metrics: 1) the distance of charge transfer (D_{CT}), and 2) the amount of charge transferred (q_{CT}). These two metrics reveal that there is a greater CT character in the excited states of DIDOBNA-N compared to that of MesB-DIDOBNA-N (Tables S1–S3, Supporting Information) despite their similar difference density patterns. The magnitude of the CT character of DIDOBNA-N is still modest compared to conventional D–A TADF emitters, with D_{CT} reported to be 1.1 Å here while typical D–A TADF emitters show D_{CT} of >1.6 Å.[34] Notably, the orbital types for the T_2 states of both compounds are different from those of S_1 and so spin–orbit coupling is expected to be non-negligible.

The electrochemical properties of both emitters were investigated by cyclic voltammetry (CV) and differential pulse voltammetry (DPV) in deaerated DCM with 0.1 M tetra-n-butylammonium hexafluorophosphate as the supporting electrolyte (**Figure 4**a). The oxidation potential, E_{ox}, determined from the peak value of the first oxidation wave of the DPV curve is 1.14 and 1.39 V vs saturated calomel electrode (SCE), respectively, for DIDOBNA-N and MesB-DIDOBNA-N, which translate to respective HOMO levels of −5.48 and −5.73 eV. This is in line with the DFT calculations that predict a stabilization of the HOMO energy level of MesB-DIDOBNA-N compared to DIDOBNA-N. For DIDOBNA-N, there was a second oxidation peak in the DPV at 1.25 V. The reduction potential, E_{red}, determined from the peak value of the first reduction wave of the DPV curve is −1.94 and −2.10 V vs SCE, respectively, for DIDOBNA-N and MesB-DIDOBNA-N, which correspond to respective LUMO levels of −2.40 and −2.24 eV. The DFT calculations corroborate the trend in LUMO levels. The LUMO energy level of DIDOBNA-N is similar to other reported deep-blue emitters having a DOBNA fragment.[18,21,36] Reductions for both emitters were broad, in the case of DIDOBNA-N a second reduction peak appeared at −2.10 V, which is likely due to the reduction of the second DOBNA unit. The electrochemical band gap is calculated to be 3.08 and 3.49 eV, respectively, for DIDOBNA-N and MesB-DIDOBNA-N. Moving from DIDOBNA-N to MesB-DIDOBNA-N, the addition of the B-Mes unit resulted in a destabilization of the LUMO by 0.16 eV and a stabilization of the HOMO by 0.25 eV. The increasing bandgap from DIDOBNA-N

© 2023 The Authors. Advanced Materials published by Wiley-VCH GmbH

15214095, 2023, 33, Downloaded from https://onlinelibrary.wiley.com/doi/10.1002/adma.202300997 by Universite De Mons (Umons), Wiley Online Library on [21/08/2023]. See the Terms and Conditions (https://onlinelibrary.wiley.com/terms-and-conditions) on Wiley Online Library for rules of use; OA articles are governed by the applicable Creative Commons License

to MesB-DIDOBNA-N is consistent with the trend predicted by DFT.

The photophysical properties were studied by measurements of absorption and photoluminescence (PL), PL quantum yield (Φ_{PL}), and time-resolved PL in 10^{-6} M THF. Figure 4b shows the absorption and PL properties of DIDOBNA-N and MesB-DIDOBNA-N and these together with other photophysical data are collated in **Table 1**. There is excellent agreement between the experimental and simulated absorption spectra (Table S4 and Figure S17, Supporting Information). Intense absorption bands were noted for DIDOBNA-N and MesB-DIDOBNA-N around 250 nm, reflected in the molar absorptivity (ϵ) values of 92×10^3 and 61×10^3 M^{-1} cm^{-1}, respectively. An intense band at 340 nm ($\epsilon = 79 \times 10^3$ M^{-1} cm^{-1}) was observed for MesB-DIDOBNA-N, which has been assigned to a SRCT state as calculations predict a similar alternating increasing/decreasing electron density pattern to S_1 (Figure S17, Supporting Information). For DIDOBNA-N there is an intense band at 384 nm ($\epsilon = 66 \times 10^3$ M^{-1} cm^{-1}), a feature also observed in the absorption spectra of other systems containing DOBNA fragments.[18,20,36a] The lowest energy absorption band in DIDOBNA-N is redshifted compared to that in MesB-DIDOBNA-N, which aligns with the predicted SCS-CC2 calculations (vide supra). The intensity at the lowest energy absorption band is higher for DIDOBNA-N than MesB-DIDOBNA-N. This is qualitatively consistent with the predicted higher oscillator strength of the S_1 and S_2 states of DIDOBNA-N compared to those of MesB-DIDOBNA-N, where the oscillator strength is weak (<0.1) for S_1.

The PL spectra in solution at room temperature reveal deep-blue and near-UV emission (Figure 4b) for DIDOBNA-N and MesB-DIDOBNA-N, respectively. DIDOBNA-N shows an unstructured emission peaking at λ_{PL} = 426 nm and a moderate FWHM of 43 nm (0.29 eV). MesB-DIDOBNA-N emits in the near-UV at λ_{PL} = 399 nm, with a very small FWHM of 23 nm (0.17 eV); and a low energy shoulder at 417 nm. This emission is narrower than that reported for DOBNA (λ_{PL} = 398 nm, FWHM = 34 nm in DCM, Figure 1).[15] We simulated the vibronically-resolved emission spectrum (see Figure S18, Supporting Information) within the displaced undistorted harmonic oscillator model within the Thermal Vibration Correlation Functional formalism as implemented in MOMAP/2021A,[39] considering vibrational modes computed at the PBE0/6-31G(d,p) level for MesB-DIDOBNA-N in THF (see Supporting Information for further information on the methodology). We observed that it is composed of one main band and a lower energy side band shifted by ≈0.18 eV from the main band corresponding to the 417 nm shoulder of the experimental emission spectrum. The main band is essentially broadened by a 65 cm^{-1} twisting mode distorting the molecular core from its planarity (see Figure S18b, Supporting Information) while the side band arises from a 1389 cm^{-1} asymmetric stretching mode (see Figure S18b, Supporting Information) responsible for the localization of the difference density of the S_1 optimized state on one side of the molecule (see Figure S19b, Supporting Information). The redshifted emission of DIDOBNA-N compared to MesB-DIDOBNA-N was predicted by SCS-CC2 calculations performed on top of the S_1-optimized geometry obtained at the TDA-PBE0/6-31G(d,p) level of theory considering THF as the solvent, to align with the experimental conditions (TableS5, Supporting Information). The

Table 1. Photophysical properties of DIDOBNA-N and MesB-DIDOBNA-N.

Compound	Medium	λ_{Abs} [c] [nm]	λ_{PL} [d] [nm]	FWHM [e] [nm]	E_{S1} [f] [eV]	E_{T1} [f] [eV]	ΔE_{ST} [h] [eV]	Φ_{PL} [i] [%]	τ_p [j] [ns]	τ_d [j] [µs]	k_{ISC} [k] [s^{-1}]	k_{RISC} [k] [s^{-1}]	k_{s_r} [k] [s^{-1}]	k_{s_nr} [k] [s^{-1}]
DIDOBNA-N	Sol. [a]	384 (66)	426	43	3.08 [g]	2.86 [g]	0.22	73 [a]	3.07	–	–	–	2.38×10^8	–
	Film [b]	–	444	64	3.12	2.89	0.23	80.8 [b]	6.83	13.7	1.55×10^7	3.14×10^4	1.19×10^8	2.77×10^7
MesB-DIDOBNA-N	Sol. [a]	388 (26)	399	23	3.17 [g]	2.93 [g]	0.24	33 [a]	2.63	–	–	–	1.25×10^8	–
	Film [b]	–	402	19	3.18	2.94	0.24	74.7 [b]	5.09	95.9	6.18×10^7	9.81×10^3	1.47×10^8	4.97×10^7

[a] In THF solutions (10^{-6} M); [b] Measured in evaporated thin films consisting of 1.5 wt% emitter in TSPO1 host under vacuum. λ_{exc} = 280 nm; [c] Lowest energy absorbance peak, absorptivity (ϵ) in parenthesis (10^4 $M^{-1}Cm^{-1}$); [d] Steady-state emission maximum at 300 K. λ_{exc} = 365 nm; [e] FWHM of emission peak; [f] S_1 and T_1 energies were obtained from the onsets of the respective prompt fluorescence (delay: 1 ns; gate time: 100 ns) and phosphorescence spectra (delay: 1 ms; gate time: 9 ms) at 77 K. λ_{exc} = 343 nm; [g] Solution samples for ΔE_{ST} measurements were prepared in 2-MeTHF (10^{-6} M); [h] $\Delta E_{ST} = E(S_1) - E(T_1)$; [i] Relative Φ_{PL} in solutions were measured by a comparative method using quinine sulfate as a standard (Φ_r = 54.6% in 1 N H_2SO_4),[37] while absolute Φ_{PL} of the thin films were measured using an integrating sphere; [j] Prompt and delayed lifetimes were obtained by TCSPC and MCS, respectively. λ_{exc} = 378 nm; [k] Intersystem and reverse intersystem crossing rates were calculated using the steady-state approximation method as described in the literature.[38]

© 2023 The Authors. Advanced Materials published by Wiley-VCH GmbH

15214095, 2023, 33, Downloaded from https://onlinelibrary.wiley.com/doi/10.1002/adma.202300997 by Universite De Mons (Umons), Wiley Online Library on [21/08/2023]. See the Terms and Conditions (https://onlinelibrary.wiley.com/terms-and-conditions) on Wiley Online Library for rules of use; OA articles are governed by the applicable Creative Commons License

Stokes shifts of DIDOBNA-N and MesB-DIDOBNA-N are 42 and 11 nm, respectively, reflecting the small reorganization energies in the excited states of these two compounds, especially for MesB-DIDOBNA-N. We investigated the nature of the excited states by measuring the emission in solvents of varying polarity (Table S6 and Figure S20, Supporting Information). In low polarity solvents from toluene to DCM, both MesB-DIDOBNA-N and DIDOBNA-N undergo a modest redshift of 6 and 18 nm, respectively. The larger bathochromic shift in the latter reflects the greater CT content of DIDOBNA-N. This suggests both emitters have SRCT S_1 states, in line with their calculated difference density plots (vide supra). Despite its SRCT excited state the FWHM of DIDOBNA-N is unusually large compared to other MR-TADF emitters, with its broadness assigned to the wider range of available conformers, this has been reported previously for some flexible MR-TADF emitters.[40] A much more significant redshifting and broadening of the emission is observed in the high-polarity solvents DMF and DMSO (Table S6 and Figure S20, Supporting Information). This is due to the stabilization of a previously higher-lying CT state below the SRCT state, which now dominates the emission. This behavior, along with the observed dual SRCT and CT emission, have been observed in other MR-TADF emitters.[41] The singlet-triplet energy gaps (ΔE_{ST}), determined from the difference in energy of the onsets of the prompt fluorescence and phosphorescence spectra at 77 K in 2Me-THF glass (Figure S21, Supporting Information) are 0.22 and 0.24 eV, respectively, for DIDOBNA-N and MesB-DIDOBNA-N, values in line with the predicted ones (Figure 3b). DIDOBNA-N and MesB-DIDOBNA-N possess similar triplet energy levels of 2.86 and 2.93 eV, respectively. The Φ_{PL} in degassed dilute THF solutions is 73% and 33% for DIDOBNA-N and MesB-DIDOBNA-N, respectively. The Φ_{PL} values decrease to 61% and 26%, respectively, upon exposure to air. Both emitters showed a small decrease in Φ_{PL} upon exposure to air that can be attributed to singlet quenching[42] as there was no delayed emission detected in the transient PL measurements (Figure S22, Supporting Information). The measured k_r in degassed THF solutions are 2.38 and 1.40×10^8 s^{-1} for DIDOBNA-N and MesB-DIDOBNA-N, respectively. Using the optimized S_1 in THF, the calculated k_r values from SCS-CC2 are consistent with this trend (Table S5, Supporting Information).

To avoid possible intermolecular interactions or concentration-induced quenching, both molecules were doped into high triplet energy (E_T) hosts at a low doping concentration. Three high triplet energy widely used phosphine-oxide-based hosts, TSPO1, DPEPO, and PPT, were compared, among which TSPO1 showed the best performance in terms of Φ_{PL} (Table S7, Supporting Information) and device EQE that are due to its high E_T (3.36 eV) and tendency to better bipolar carrier transport than the other host materials.[43] The Φ_{PL} values for 1.5 wt% doped TSPO1 films containing DIDOBNA-N and MesB-DIDOBNA-N are 81% and 75%, respectively (Table S7, Supporting Information). The Φ_{PL} value of MesB-DIOBNA-N is higher in thin film than in solution, which is likely the result of suppressed vibrations and consequently slower nonradiative decay processes from the emitter in the rigid host matrix. **Figure 5**a shows the steady-state photophysical properties of evaporated thin films with a doping concentration of 1.5 wt% in TSPO1. DIDOBNA-N shows a deep-blue emission at 444 nm with FWHM of 64 nm (0.38 eV), which is redshifted and broader than that in dilute THF solution (λ_{PL} = 426 nm and FWHM = 43 nm (0.29 eV)). The redshift and spectral broadening of the emission are attributed to the polarization effect of the host matrix on the different excited state properties.[44] By contrast, MesB-DIDOBNA-N showed negligible changes in its steady-state PL spectrum in the thin film (λ_{PL} at 402 nm and a FWHM of only 19 nm (0.15 eV)) compared to that in solution (λ_{PL} = 399 nm and FWHM = 23 nm (0.17 eV)). The observed narrowband emission spectra of DIDOBNA-N and MesB-DIDOBNA-N translate to deep-blue and near-UV emission at CIE coordinates of (0.150, 0.063), and (0.165, 0.022), respectively, which match well the blue CIE coordinates of BT.709 and BT.2020 standards for HDTV and UHDTV, that is, (0.150, 0.06), and (0.131, 0.046), respectively. The S_1/T_1 energies for DIDOBNA-N and MesB-DIDOBNA-N in 1.5 wt% doped TSPO1 films were determined from the onsets of the respective prompt fluorescence and phosphorescence spectra at 77 K, which are 3.12 eV/2.89 eV and 3.18 eV/2.94 eV, respectively. The corresponding ΔE_{ST} values are 0.23 and 0.24 eV, respectively, which are consistent with those determined in 2-MeTHF.

We next acquired temperature-dependent time-resolved PL decays of the TSPO1 doped films using multichannel scaling (MCS). The decays, which are presented in Figure 5b,c, show both prompt (PF) and delayed fluorescence (DF) components for both emitters. Whereas the prompt component exhibited negligible temperature dependence, the intensity of the DF decreased significantly with decreasing temperature, behavior that is characteristic of TADF compounds. The lifetimes of both PF and DF were estimated by fitting the decays with a multi-exponential decay fitting (for details of the fitting of the decays see Page S4, Supporting Information). The prompt, τ_p, and delayed, τ_d, lifetimes are τ_p/τ_d = 6.83 ns/13.72 µs and 5.09 ns/95.91 µs for DIDOBNA-N and MesB-DIDOBNA-N, respectively. Both emitters exhibited high radiative rates in the order of 10^8 s^{-1} (Table 1); however, RISC rates are slow at 3.14×10^4 and 9.81×10^3 s^{-1}, respectively, for DIDOBNA-N and MesB-DIDOBNA-N; deep-blue D–A DOBNA-containing TADF compounds have been reported to show k_{RISC} on average on the order of 10^6 s^{-1}.[18–24,45] More generally, deep-blue MR-TADF compounds rarely show k_{RISC} above 10^4 s^{-1}.[46] The k_{RISC} for DOBNA was reported to be 1.6×10^4 s^{-1} in 1 wt% PMMA,[16] which is just slightly faster than that of MesB-DIDOBNA-N (9.81×10^3 s^{-1}).

2.1. Device Performance

The potential of the emitters in deep-blue and near-UV electroluminescent (EL) devices was next assessed. To confine the excitons on the emitter, the high triplet energy material TSPO1 was selected as the host. Since TSPO1 has a dominant electron-transport character, the recombination zone inside the emission layer (EML) is located near the interface between the emission layer (EML) and the hole transport layer (HTL). To avoid exciton loss into the HTL, an exciton blocking layer of 10 nm thick CzSi [(9-(4-*tert*-butylphenyl)-3,6-bis(triphenylsilyl)-9*H*-carbazole, E_T = 3.0 eV][47] was inserted between the EML and HTL.

The optimized device structure was: indium tin oxide (ITO)/hexaazatriphenylenehexacarbonitrile (HAT-CN,

© 2023 The Authors. Advanced Materials published by Wiley-VCH GmbH

15214095, 2023, 33, Downloaded from https://onlinelibrary.wiley.com/doi/10.1002/adma.202306997 by Universite De Mons (Umons), Wiley Online Library on [21/08/2023]. See the Terms and Conditions (https://onlinelibrary.wiley.com/terms-and-conditions) on Wiley Online Library for rules of use; OA articles are governed by the applicable Creative Commons License

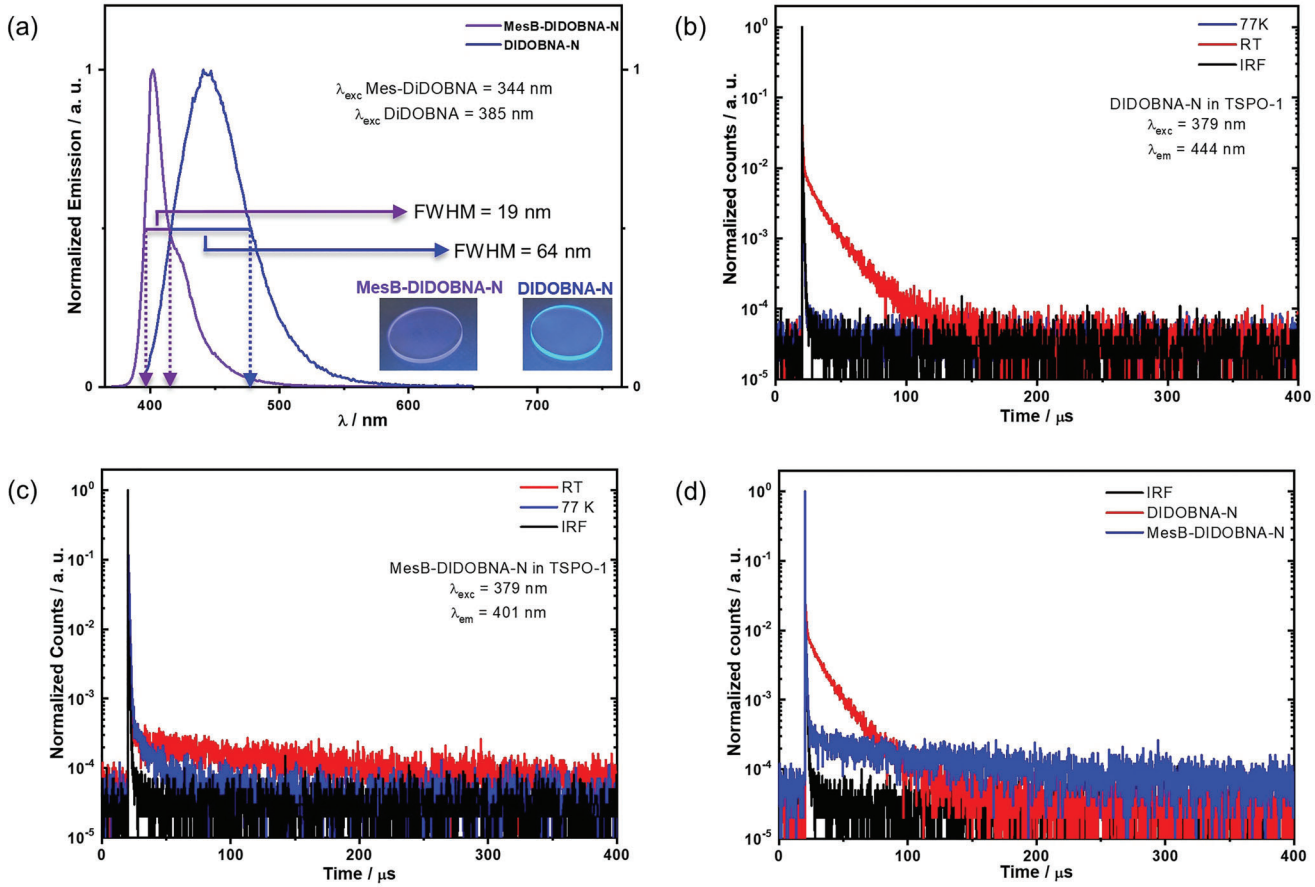

Figure 5. Co-evaporated thin film of 1.5 wt% emitter doped in TSPO1 host. a) Steady-state PL spectra at room temperature under vacuum, $\lambda_{exc.}$ (DIDOBNA-N) = 385 nm, $\lambda_{exc.}$ (MesB-DIDOBNA-N) = 344 nm; b) time-resolved PL decay at RT and 77 K of DIDOBNA-N, $\lambda_{exc.}$ = 379 nm; c) time-resolved PL decay at RT and 77 K of MesB-DIDOBNA-N, $\lambda_{exc.}$ = 379 nm; d) decay of emission signal at RT plotted together with IRF signal.

5 nm)/*N,N′*-di(1-naphthyl)-*N,N′*-diphenyl-(1,1′-biphenyl)-4,4′-diamine (NPB, 40 nm)/tris(4-carbazoyl-9-ylphenyl)amine (TCTA, 10 nm)/CzSi (10 nm)/MesB-DIDOBNA-N or DIDOBNA-N :TSPO1 (c_D, 20 nm)/TSPO1 (10 nm)/1,3,5-tris(3-pyridyl-3-phenyl)benzene (TmPyPB, 20 nm)/LiF (0.8 nm)/Al (100 nm), where HAT-CH, NPB, TCTA, CzSi, TSPO1, TmPyPB, and LiF are the hole-injection (HIL), HTL, electron-blocking (EBL), exciton-blocking, hole-blocking (HBL), electron-transport (ETL), and electron-injection layers (EIL), respectively. The device structure and energy levels of each layer are illustrated in Figure S23, Supporting Information.

We first investigated the device performance with DIDOBNA-N as the emitter (**Table 2**). The OLED with c_D of 1.5 wt% showed deep-blue, unstructured EL emission at 429 nm with FWHM of 70 nm, resulting in CIE coordinates of (0.152, 0.073), close to the NTSC standard of (0.14, 0.08), **Figure 6**a. The EL spectrum was similar to the PL spectrum in its dilute THF solution, though the FWHM became slightly broader, possibly due to the polarity of the host. The maximum EQE (EQE_{max}) reached as high as 15.2%, which is the highest EQE_{max} among the reported OLEDs based on polycyclic aromatic hydrocarbon emitters with λ_{EL} < 430 nm (Figure 6d); the efficiency roll-off was

Table 2. Device performance of DIDOBNA-N and MesB-DIDOBNA-N.

Emitter	c_D [wt%]	V_{on} [V]	λ_{EL} [nm]	FWHM [nm]	CIE (*x*,*y*)	EQE_{max} ($EQE_{100cd\ m^{-2}}$) [%]	PE_{max} ($PE_{100\ cd\ m^{-2}}$) [lm W^{-1}]
DIDOBNA-N	1.5	4.2	429	70	(0.152, 0.073)	15.2 (3.8)	6.5 (1.05)
MesB-DIDOBNA-N	1.5	4.5	402	22	(0.165, 0.044)	9.3 (–)	1.1 (–)
	3.0	4.5	404	25	(0.166, 0.045)	11.3 (–)	1.8 (–)
	5.0	4.2	405	31	(0.165, 0.055)	13.6 (–)	3.1 (–)
MesB-DIDOBNA-N[a)]	3.0	4.1	402	21	(0.170, 0.049)	16.2 (3.5)	2.7 (0.35)

[a)] Co-host device with 1:1 CzSi:TSPO1. The performance of devices with other co-host ratios is summarized in Table **S9**, Supporting Information.

 © 2023 The Authors. Advanced Materials published by Wiley-VCH GmbH

15214095, 2023, 33, Downloaded from https://onlinelibrary.wiley.com/doi/10.1002/adma.202300997 by Universite De Mons (Umons), Wiley Online Library on [21/08/2023]. See the Terms and Conditions (https://onlinelibrary.wiley.com/terms-and-conditions) on Wiley Online Library for rules of use; OA articles are governed by the applicable Creative Commons License

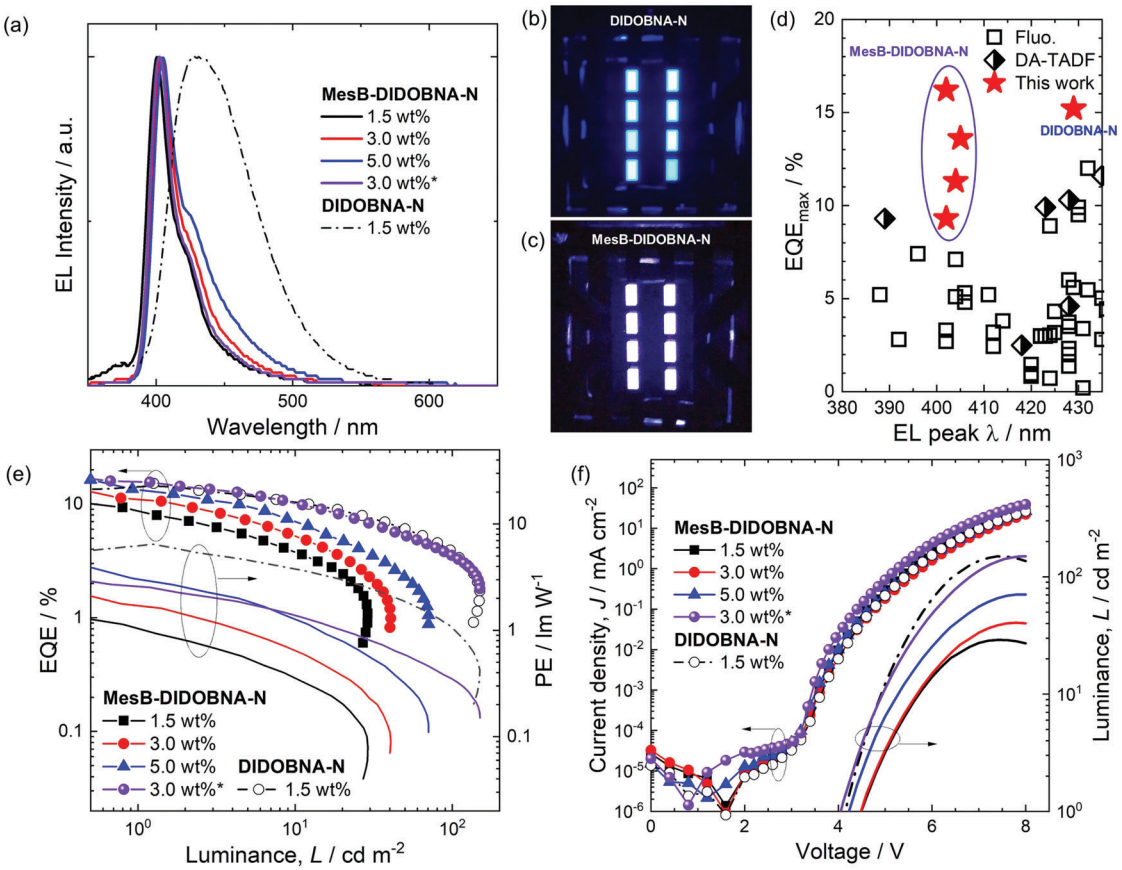

Figure 6. OLED device data for MesB-DIDOBNA-N and DIDOBNA-N as emitters. a) EL spectrum of both emitters at 5 V. b,c) Images of operating devices of DIDOBNA-N and MesB-DIDOBNA-N, respectively, under 5 V. d) Summary of literature-reported device efficiencies with λ_{EL} < 430 nm and a cross-comparison to the efficiencies reported here. e) Dependence of external quantum efficiency (EQE) and power efficiency (PE) on the luminance. f) Current density–voltage–luminance (*J*–*V*–*L*) characteristics of the device. *Co-host device with 1:1 CzSi:TSPO1.

severe and the EQE decreased to 3.8% at 100 cd m^{-2}. Large efficiency roll-off and low maximum luminance (L_{max}) in deep-blue OLEDs are not uncommon, which have been attributed to significant bimolecular interactions at large current density, such as singlet-triplet annihilation, triplet-triplet annihilation and triplet-polaron quenching, and low luminosity function value at short wavelength, respectively.[48] In addition, the high triplet energy of the emitters necessitates the use of hosts with even higher triplet energies. This implies that the hosts employed have very large HOMO–LUMO gaps, rendering the energy level alignment between adjacent layers difficult. In other words, it is challenging to keep balanced bipolar carrier distribution inside the EML of deep-blue OLEDs.

With the exact same device structure and doping concentration of 1.5wt%, the MesB-DIDOBNA-N device showed extraordinary EL performance (Figure 6a), with near-UV narrowband emission at 402 nm and a FWHM of 22 nm. The nearly identical EL spectrum with the PL spectrum in THF solution indicates that the device also emits from the same SRCT state. The device EQE_{max} of 9.3% ranks the OLED amongst the highest of reported devices with λ_{EL} at 400 nm (Figure 6d).[7,8,30]

Recognizing the similar issues of large efficiency roll-off and low L_{max} in the two devices, two approaches were adopted to address these facets of the near-UV MesB-DIDOBNA-N device performance. First, the doping concentration (c_D) of MesB-DIDOBNA-N was optimized from 1.5, 3.0, to 5.0 wt%. Considering the HOMO/LUMO levels of the emitter, MesB-DIDOBNA-N (5.73 eV/2.24 eV), and the host, TSPO1 (6.79 eV/2.50 eV), holes and electrons are mainly transported via the emitter and the host molecules, respectively. In other words, the injected holes are mostly trapped on the emitters, which then capture the mobile electrons hopping via the transporting sites of the TSPO1 host in a trap-assisted recombination mechanism. Therefore, an increase of the emitter doping concentration should improve the bipolar carrier transport, resulting in a higher probability of electron–hole recombination. This was indeed observed in our study. As c_D increased from 1.5, 3.0 to 5.0 wt%, the EQE_{max} increased from 9.3 to 11.3 and 13.6%, respectively (Figure 6e). In addition, luminance at 8 V was improved from 30, 40, to 70 cd m^{-2}, respectively (Figure 6f), though these are still less than 100 cd m^{-2} (Table 2).

Nevertheless, the increased doping concentration could undermine the color purity due to the increased likelihood of intermolecular interactions of the emitter molecules. With increasing c_D, the λ_{EL} redshifted slightly to 404 (3 wt%) and 405 nm (5 wt%) while the FWHM increased to 25 and 31 nm, respectively.

© 2023 The Authors. Advanced Materials published by Wiley-VCH GmbH

15214095, 2023, 33, Downloaded from https://onlinelibrary.wiley.com/doi/10.1002/adma.202300997 by Universite De Mons (Umons), Wiley Online Library on [21/08/2023]. See the Terms and Conditions (https://onlinelibrary.wiley.com/terms-and-conditions) on Wiley Online Library for rules of use; OA articles are governed by the applicable Creative Commons License

The spectral broadening resulted mainly from the increased intensity of the low-energy shoulder peak at 430 nm. Despite these undesired spectral changes with increasing c_D, the devices nonetheless showed extraordinary color purity, with CIE coordinates of (0.165, 0.044), (0.166, 0.045) and (0.166, 0.055) for the MesB-DIDOBNA-N OLEDs with c_D of 1.5, 3.0 and 5wt%, respectively. Those values, especially the device with c_D of 3.0 wt%, are very close to the BT.2020 standard for the primary blue color of UHDTV (CIE coordinates of (0.131, 0.046)).

Second, a co-host strategy was applied to further improve the bipolar carrier transport of the 3.0 wt% doped MesB-DIDOBNA-N device. Due to the scarcity of the high triplet energy hosts, hole transport CzSi and electron transport TSPO1 hosts were used as a 1:1 mixture. No new emission peaks were observed from the CzSi:TSPO1 co-host, implying no interaction between two components (i.e., the co-host acts only a mixed host system). At 3.0 wt% doping of MesB-DIDOBNA-N in the 1:1 co-host, narrowband near-UV PL at λ_{PL} of 402 nm was observed (Table 2). The Φ_{PL} of the 3.0 wt% doped films in CzSi, 1:1 CzSi:TSPO1 and TSPO1 were 66%, 73% and 73%, respectively, which were slightly lower than the 75% of the 1.5 wt% doped film in TSPO1. Gratifyingly, the device performance was significantly improved (Figure 6, and Figure S24, Supporting Information). Not only was the EQE_{max} (EQE_{100}) increased to 16.2% (3.5%), but L_{max} reached 200 cd m^{-2}, validating the effectiveness of the co-host strategy. In addition, the turn-on voltage (V_{on}) was reduced from 4.5 to 4.1 V, implying a lowered injection barrier into the EML. On the other hand, the EL properties of the co-host device were almost unaffected with λ_{EL} at 402 nm, FWHM of 22 nm, and CIE coordinates of (0.170, 0.049). We note that the device lifetime at 100 cd m^{-2} was short (qualitatively less than 1 h), such a short device lifetime is a long-standing issue of blue OLEDs and is largely attributed to the unstable high triplet energy host.[49] Nevertheless, after the two-step optimization, the MesB-DIDOBNA-N OLED has the highest EQE_{max} among all the reported fluorescent and TADF devices with λ_{EL} around 400 nm (Figure 6d, and Table S9, Supporting Information).

3. Conclusions

Two new easy-to-access MR-TADF emitters have been synthesized in good yields. DIDOBNA-N showed efficient deep-blue emission and TADF in 1.5 wt% TSPO1 films (λ_{PL} = 444 nm, FWHM = 64 nm, Φ_{PL} = 81%, τ_d = 23 µs). The electroluminescence is blueshifted (λ_{EL} = 429 nm, FWHM = 70 nm, CIE_y = 0.073), corresponding well to the NTSC standard of (0.14, 0.08). The OLED shows an excellent EQE_{max} of 15.3%, which is the highest reported for a deep-blue emitter with a λ_{EL} < 430 nm.[7,21,30] MesB-DIDOBNA-N was obtained from DIDOBNA-N in one step by installing a bridging mesitylated borane unit, the result of this structural change was a significantly blueshifted and narrowed emission. This compound represents a rare example of a non-triangulene type π-extended near-UV MR-TADF emitter. The molecular design utilized two electronically distinct acceptor boron atoms in combination with mixed donor nitrogen, and oxygen atoms. This emitter shows narrowband pure near-UV emission in the 1.5 wt% TSPO1 film (λ_{PL} = 402 nm, FWHM = 19 nm, Φ_{PL} = 75%, τ_d = 133 µs), which translated into record-setting near-UV MR-TADF OLED $EQE_{max/100}$ of 16.2%/3.5%, (λ_{EL} = 402 nm, FWHM = 21 nm, CIE_y = 0.049). The EL from the MesB-DIDOBNA-N device is the bluest of all the MR-TADF OLEDs reported to date.[7,8,30] The results from our device study are promising not only as near-UV light sources but more importantly showcase materials design for high-performance near-UV emitters that can be used in sensing, photochemistry, high-density information storage, medicine, and sterilization.

Supporting Information

Supporting Information is available from the Wiley Online Library or from the author.

Acknowledgements

S.M.S. and L.Z. contributed equally to this work. This project has received funding from the European Union's Horizon 2020 research and innovation programme under the Marie Skłodowska Curie grant agreement No 838885 (NarrowbandSSL). S.M.S. acknowledges support from the Marie Skłodowska-Curie Individual Fellowship (grant agreement No 838885 NarrowbandSSL). The authors would like to thank the Leverhulme Trust (RPG-2016-047) for financial support. E.Z.-C. and I.D.W.S. acknowledge support from EPSRC (EP/L017008, EP/P010482/1). Computational resources have been provided by the Consortium des Équipements de Calcul Intensif (CÉCI), funded by the Fonds de la Recherche Scientifiques de Belgique (F. R. S.-FNRS) under Grant No. 2.5020.11, as well as the Tier-1 supercomputer of the Fédération Wallonie-Bruxelles, infrastructure funded by the Walloon Region under the grant agreement n1117545. Y.O. acknowledges funding by the Fonds de la Recherche Scientifique-FNRS under Grant n°F.4534.21 (MIS-IMAGINE). D.B. is a FNRS Research Director. G.R. acknowledges a grant from the "Fonds pour la formation à la Recherche dans l'Industrie et dans l'Agriculture" (FRIA) of the FRS-FNRS.

Conflict of Interest

The authors declare no conflict of interest.

Data Availability Statement

The data that support the findings of this study are openly available in the St Andrews research portal at https://doi.org/10.17630/90d001cb-c3d4-497b-b8b8-95ead28cd88e.

Keywords

boron, deep-blue emitters, multiresonant thermally activated delayed fluorescence (MR-TADF), near-UV emitters, organic light-emitting diodes (OLEDs)

Received: February 1, 2023
Revised: April 26, 2023
Published online: July 6, 2023

[1] G. Hong, X. Gan, C. Leonhardt, Z. Zhang, J. Seibert, J. M. Busch, S. Bräse, *Adv. Mater.* **2021**, *33*, 2005630.
[2] In *BT.2020-2 (10/2015)*, Vol. *2015-10*, International Telecommunication Union, Geneva, Switzerland **2015**.

© 2023 The Authors. Advanced Materials published by Wiley-VCH GmbH

15214095, 2023, 33, Downloaded from https://onlinelibrary.wiley.com/doi/10.1002/adma.202300997 by Universite De Mons (Umons), Wiley Online Library on [21/08/2023]. See the Terms and Conditions (https://onlinelibrary.wiley.com/terms-and-conditions) on Wiley Online Library for rules of use; OA articles are governed by the applicable Creative Commons License

[3] a) X. Cai, S.-J. Su, *Adv. Funct. Mater.* **2018**, *28*, 1802558; b) H. Fu, Y.-M. Cheng, P.-T. Chou, Y. Chi, *Mater. Today* **2011**, *14*, 472.
[4] a) M. Y. Wong, E. Zysman-Colman, *Adv. Mater.* **2017**, *29*, 1605444; b) N. Aizawa, A. Matsumoto, T. Yasuda, *Sci. Adv.* **2021**, *7*, eabe5769.
[5] H. Lee, D. Karthik, R. Lampande, J. H. Ryu, J. H. Kwon, *Front. Chem.* **2020**, *8*, 373.
[6] a) S. M. Suresh, D. Hall, D. Beljonne, Y. Olivier, E. Zysman-Colman, *Adv. Funct. Mater.* **2020**, *30*, 1908677; b) J.-W. Huang, Y.-C. Hsu, X. Wu, S. Wang, X.-Q. Gan, W.-Q. Zheng, H. Zhang, Y.-Z. Gong, W.-Y. Hung, P.-T. Chou, W. Zhu, *J. Mater. Chem. C* **2022**, *10*, 7866.
[7] J. M. Ha, S. H. Hur, A. Pathak, J.-E. Jeong, H. Y. Woo, *NPG Asia Mater.* **2021**, *13*, 53.
[8] S. Chen, H. Xu, *Chem. Soc. Rev.* **2021**, *50*, 8639.
[9] J. Shinar, R. Shinar, *J. Phys. D: Appl. Phys.* **2008**, *41*, 133001.
[10] a) D. S. Thakare, S. K. Omanwar, P. L. Muthal, S. M. Dhopte, V. K. Kondawar, S. V. Moharil, *Phys. Status Solidi* **2004**, *201*, 574.
[11] H. V. Santen, J. H. M. Neijzen, *Jpn. J. Appl. Phys.* **2003**, *42*, 1110.
[12] L. T. T. Nhung, H. Nagata, A. Takahashi, M. Aihara, T. Okamoto, T. Shimohata, K. Mawatari, M. Akutagawa, Y. Kinouchi, M. Haraguchi, *J. Med. Invest.* **2012**, *59*, 53.
[13] a) H. Zhang, G. Li, X. Guo, K. Zhang, B. Zhang, X. Guo, Y. Li, J. Fan, Z. Wang, D. Ma, B. Z. Tang, *Angew. Chem., Int. Ed.* **2021**, *60*, 22241; b) J. Chen, H. Liu, J. Guo, J. Wang, N. Qiu, S. Xiao, J. Chi, D. Yang, D. Ma, Z. Zhao, B. Z. Tang, *Angew. Chem., Int. Ed.* **2022**, *61*, e202116810.
[14] Y. Xu, P. Xu, D. Hu, Y. Ma, *Chem. Soc. Rev.* **2021**, *50*, 1030.
[15] H. Hirai, K. Nakajima, S. Nakatsuka, K. Shiren, J. Ni, S. Nomura, T. Ikuta, T. Hatakeyama, *Angew. Chem., Int. Ed.* **2015**, *54*, 13581.
[16] N. Ikeda, S. Oda, R. Matsumoto, M. Yoshioka, D. Fukushima, K. Yoshiura, N. Yasuda, T. Hatakeyama, *Adv. Mater.* **2020**, *32*, 2004072.
[17] D. Liang, Y. Peng, Y. Fu, M. J. Shearer, J. Zhang, J. Zhai, Y. Zhang, R. J. Hamers, T. L. Andrew, S. Jin, *ACS Nano* **2016**, *10*, 6897.
[18] D. H. Ahn, S. W. Kim, H. Lee, I. J. Ko, D. Karthik, J. Y. Lee, J. H. Kwon, *Nat. Photonics* **2019**, *13*, 540.
[19] H. J. Kim, M. Godumala, S. K. Kim, J. Yoon, C. Y. Kim, H. Park, J. H. Kwon, M. J. Cho, D. H. Choi, *Adv. Opt. Mater.* **2020**, *8*, 1902175.
[20] H. Lim, H. J. Cheon, S.-J. Woo, S.-K. Kwon, Y.-H. Kim, J.-J. Kim, *Adv. Mater.* **2020**, *32*, 2004083.
[21] J. Hwang, C. W. Koh, J. M. Ha, H. Y. Woo, S. Park, M. J. Cho, D. H. Choi, *ACS Appl. Mater. Interfaces* **2021**, *13*, 61454.
[22] Y. Lee, J.-I. Hong, *Adv. Opt. Mater.* **2021**, *9*, 2100406.
[23] H.-J. Tan, G.-X. Yang, Y.-L. Deng, C. Cao, J.-H. Tan, Z.-L. Zhu, W.-C. Chen, Y. Xiong, J.-X. Jian, C.-S. Lee, Q.-X. Tong, *Adv. Mater.* **2022**, *34*, 2200537.
[24] Y. Gan, X. Peng, W. Qiu, L. Wang, D. Li, W. Xie, D. Liu, M. Li, J. Lin, S.-J. Su, *Chem. Eng. J.* **2022**, *430*, 133030.
[25] H. L. Lee, W. J. Chung, J. Y. Lee, *Small* **2020**, *16*, 1907569.
[26] D. Hall, K. Stavrou, E. Duda, A. Danos, S. Bagnich, S. Warriner, A. M. Z. Slawin, D. Beljonne, A. Köhler, A. Monkman, Y. Olivier, E. Zysman-Colman, *Mater. Horiz.* **2022**, *9*, 1068.
[27] S. M. Suresh, E. Duda, D. Hall, Z. Yao, S. Bagnich, A. M. Z. Slawin, H. Bässler, D. Beljonne, M. Buck, Y. Olivier, A. Köhler, E. Zysman-Colman, *J. Am. Chem. Soc.* **2020**, *142*, 6588.
[28] K. Stavrou, S. M. Suresh, D. Hall, A. Danos, N. Kukhta, A. Slawin, S. Warriner, D. Beljonne, Y. Olivier, A. Monkman, E. Zysman-Colman, *Adv. Opt. Mater.* **2022**, *10*, 2200688.
[29] S. Madayanad Suresh, L. Zhang, D. Hall, C. Si, G. Ricci, T. Matulaitis, A. M. Z. Slawin, S. Warriner, Y. Olivier, I. D. W. Samuel, E. Zysman-Colman, *Angew. Chem., Int. Ed.* **2023**, *62*, e202215522.
[30] H. J. Kim, T. Yasuda, *Adv. Opt. Mater.* **2022**, *10*, 2201714.
[31] T. Agou, J. Kobayashi, T. Kawashima, *Org. Lett.* **2006**, *8*, 2241.
[32] D. Hall, J. C. Sancho, A. Pershin, D. Beljonne, E. Zysman-Colman, Y. Olivier, *J. Chem. Theory Comput.* **2022**, *18*, 4903.
[33] a) M. K. Etherington, J. Gibson, H. F. Higginbotham, T. J. Penfold, A. P. Monkman, *Nat. Commun.* **2016**, *7*, 13680; b) M. Hempe, N. A. Kukhta, A. Danos, M. A. Fox, A. S. Batsanov, A. P. Monkman, M. R. Bryce, *Chem. Mater.* **2021**, *33*, 3066; c) X.-F. Luo, H.-X. Ni, H.-L. Ma, Z.-Z. Qu, J. Wang, Y.-X. Zheng, J.-L. Zuo, *Adv. Opt. Mater.* **2022**, *10*, 2102513; d) V. V. Patil, H. L. Lee, I. Kim, K. H. Lee, W. J. Chung, J. Kim, S. Park, H. Choi, W.-J. Son, S. O. Jeon, J. Y. Lee, *Adv. Sci.* **2021**, *8*, 2101137.
[34] Y. Olivier, J. C. Sancho-Garcia, L. Muccioli, G. D'Avino, D. Beljonne, *J. Phys. Chem. Lett.* **2018**, *9*, 6149.
[35] N. G. Connelly, W. E. Geiger, *Chem. Rev.* **1996**, *96*, 877.
[36] a) D. Song, Y. Yu, L. Yue, D. Zhong, Y. Zhang, X. Yang, Y. Sun, G. Zhou, Z. Wu, *J. Mater. Chem. C* **2019**, *7*, 11953; b) D. H. Ahn, J. H. Maeng, H. Lee, H. Yoo, R. Lampande, J. Y. Lee, J. H. Kwon, *Adv. Opt. Mater.* **2020**, *8*, 2000102.
[37] W. H. Melhuish, *J. Phys. Chem.* **1961**, *65*, 229.
[38] Y. Tsuchiya, S. Diesing, F. Bencheikh, Y. Wada, P. L. dos Santos, H. Kaji, E. Zysman-Colman, I. D. W. Samuel, C. Adachi, *J. Phys. Chem. A* **2021**, *125*, 8074.
[39] Z. Shuai, *Chin. J. Chem.* **2020**, *38*, 1223.
[40] D. Sun, S. M. Suresh, D. Hall, M. Zhang, C. Si, D. B. Cordes, A. M. Z. Slawin, Y. Olivier, X. Zhang, E. Zysman-Colman, *Mater. Chem. Front.* **2020**, *4*, 2018.
[41] a) S. Wu, W. Li, K. Yoshida, D. Hall, S. Madayanad Suresh, T. Sayner, J. Gong, D. Beljonne, Y. Olivier, I. D. W. Samuel, E. Zysman-Colman, *ACS Appl. Mater. Interfaces* **2022**, *14*, 22341; b) J. A. Knöller, G. Meng, X. Wang, D. Hall, A. Pershin, D. Beljonne, Y. Olivier, S. Laschat, E. Zysman-Colman, S. Wang, *Angew. Chem., Int. Ed.* **2020**, *59*, 3156.
[42] J. R. Lakowicz, in *Principles of Fluorescence Spectroscopy* (Ed: J. R. Lakowicz), Springer US, Boston, MA, USA **1983**, pp. 257–301.
[43] S. O. Jeon, S. E. Jang, H. S. Son, J. Y. Lee, *Adv. Mater.* **2011**, *23*, 1436.
[44] a) T. Northey, J. Stacey, T. J. Penfold, *J. Mater. Chem. C* **2017**, *5*, 11001; b) T. Serevičius, R. Skaisgiris, J. Dodonova, I. Fiodorova, K. Genevičius, S. Tumkevičius, K. Kazlauskas, S. Juršėnas, *J. Phys. Chem. Lett.* **2022**, *13*, 1839.
[45] I. S. Park, H. Min, J. U. Kim, T. Yasuda, *Adv. Opt. Mater.* **2021**, *9*, 2101282.
[46] a) M. Nagata, H. Min, E. Watanabe, H. Fukumoto, Y. Mizuhata, N. Tokitoh, T. Agou, T. Yasuda, *Angew. Chem., Int. Ed.* **2021**, *60*, 20280; b) S. Oda, B. Kawakami, Y. Yamasaki, R. Matsumoto, M. Yoshioka, D. Fukushima, S. Nakatsuka, T. Hatakeyama, *J. Am. Chem. Soc.* **2022**, *144*, 106; c) J. Bian, S. Chen, L. Qiu, R. Tian, Y. Man, Y. Wang, S. Chen, J. Zhang, C. Duan, C. Han, H. Xu, *Adv. Mater.* **2022**, *34*, 2110547.
[47] M.-H. Tsai, T.-H. Ke, H.-W. Lin, C.-C. Wu, S.-F. Chiu, F.-C. Fang, Y.-L. Liao, K.-T. Wong, Y.-H. Chen, C.-I. Wu, *ACS Appl. Mater. Interfaces* **2009**, *1*, 567.
[48] a) B. van der Zee, Y. Li, G.-J. A. H. Wetzelaer, P. W. M. Blom, *Adv. Electron. Mater.* **2022**, *8*, 2101261; b) M. Hasan, S. Saggar, A. Shukla, F. Bencheikh, J. Sobus, S. K. M. McGregor, C. Adachi, S.-C. Lo, E. B. Namdas, *Nat. Commun.* **2022**, *13*, 254.
[49] a) S.-G. Ihn, D. Jeong, E. S. Kwon, S. Kim, Y. S. Chung, M. Sim, J. Chwae, Y. Koishikawa, S. O. Jeon, J. S. Kim, J. Kim, S. Nam, I. Kim, S. Park, D. S. Kim, H. Choi, S. Kim, *Adv. Sci.* **2022**, *9*, 2102141; b) S.-G. Ihn, N. Lee, S. O. Jeon, M. Sim, H. Kang, Y. Jung, D. H. Huh, Y. M. Son, S. Y. Lee, M. Numata, H. Miyazaki, R. Gómez-Bombarelli, J. Aguilera-Iparraguirre, T. Hirzel, A. Aspuru-Guzik, S. Kim, S. Lee, *Adv. Sci.* **2017**, *4*, 1600502.

© 2023 The Authors. Advanced Materials published by Wiley-VCH GmbH

15214095, 2023, 33, Downloaded from https://onlinelibrary.wiley.com/doi/10.1002/adma.202300997 by Universite De Mons (Umons), Wiley Online Library on [21/08/2023]. See the Terms and Conditions (https://onlinelibrary.wiley.com/terms-and-conditions) on Wiley Online Library for rules of use; OA articles are governed by the applicable Creative Commons License